Chronic Perinatal Hypoxia Delays Cardiac Maturation in a Mouse Model for Cyanotic Congenital Heart Disease

Short Title: Romanowicz, Perinatal Hypoxia Delays Cardiac Maturation

Jennifer Romanowicz, MD[1], Zaenab Dhari, MD[2], Colm Mulvany, BS[3], Devon Guerrelli, MS[2,3], Marissa Reilly, BS[3], Luther Swift, PhD[3], Nimisha Vasandani, BS[2], Manelle Ramadan, BS[3], Nobuyuki Ishibashi, MD[1,2,3,4], Nikki Gillum Posnack, PhD[1,3,4]

[1]Children's National Heart Institute, Children's National Hospital, Washington, DC

[2]Center for Neuroscience Research, Children's National Hospital, Washington, DC

[3]Sheikh Zayed Institute for Pediatric Surgical Innovation, Children's National Hospital, Washington, DC

[4]Department of Pediatrics, Department of Pharmacology and Physiology, George Washington University, Washington DC

Corresponding author:

Nikki Gillum Posnack, Ph.D.

Sheikh Zayed Institute, 6th floor, M7707

111 Michigan Avenue, NW

Washington, DC, USA 20010

Tel: (202) 476-2475, Fax: (202) 476-2475

Email: nposnack@childrensnational.org

Subject Terms: Animal Models of Human Disease, Developmental Biology, Congenital Heart Disease, Electrophysiology, Contractile Function

Abstract

Background: Compared to acyanotic congenital heart disease (CHD), cyanotic CHD has an increased risk of lifelong mortality and morbidity. These adverse outcomes may be attributed to delayed cardiomyocyte maturation, since the transition from a hypoxic fetal milieu to oxygen rich postnatal environment is disrupted. To test the hypothesis that chronic perinatal hypoxia impairs cardiac maturation and functioning, we established a rodent model that replicates hypoxic myocardial conditions spanning perinatal cardiac development as observed in cyanotic CHD.

Methods: Mouse dams were housed in hypoxia beginning at embryonic day 16, coinciding with myocardial reliance on coronary flow. Pups stayed in hypoxia until postnatal day (P)8 when cardiac development is nearly complete. Global gene expression was quantified at P8 ($n \geq 4$) and at P30 after recovering in normoxia ($n \geq 4$). Phenotypic testing included electrocardiogram (P8 $n \geq 10$, P30 $n \geq 4$), echocardiogram (P30 $n \geq 3$), and *ex-vivo* electrophysiology study (P30 n=4).

Results: Hypoxic animals were 48% smaller than controls, consistent with intrauterine growth restriction observed in cyanotic neonates. Global gene expression was grossly altered by hypoxia at P8 (1427 genes affected), including changes in ion channels, sarcomere structure, and calcium handling. Gene expression changes normalized after recovery (P30). Electrocardiograms revealed bradycardia and slowed conduction velocity in hypoxic animals at P8, which resolved after recovery (P30). Notable differences that persisted after recovery (P30) included a 65% prolongation in ventricular effective refractory period, universal sinus node dysfunction, and a 24% reduction in contractile function in animals exposed to hypoxia.

Conclusions: This is the first study to investigate the impact of chronic hypoxia on the developing heart using both pre- and postnatal periods of hypoxia. Perinatal hypoxia was associated with changes in gene expression and cardiac functioning. Persistent changes to the

electrophysiologic substrate and contractile function warrant further investigation, and may contribute to adverse outcomes observed in the cyanotic CHD population.

Key Words: congenital heart disease, cardiac development, perinatal hypoxia, mouse, animal model cardiovascular disease

Introduction

Outcomes for patients with cyanotic congenital heart disease (CHD) remain guarded despite countless advances in clinical care strategies over the last decades. CHD affects 1% of live births[1], with one quarter of CHD representing cyanotic conditions[2]. Infants with cyanotic CHD are at an 8-fold increased risk of death[2] compared to acyanotic CHD, and up to 39% of all patients with CHD develop heart failure during childhood[3]. With clinical advances, the CHD population is increasingly surviving to adulthood, leading to an increased burden of CHD-associated heart failure[4]. Despite the high incidence of morbidity and mortality in the cyanotic CHD population, the underlying risk factors are not fully understood[3].

Normal embryology of the heart directs streaming of the most highly saturated blood to the head vessels and coronary arteries. For a fetus with complex CHD, this streaming pattern is disrupted and the ascending aorta blood is desaturated[5]. Chronic hypoxic conditions in the developing heart persist after birth until definitive repair. At the time of cardiac surgery, the cyanotic myocardium has depleted endogenous antioxidants[6], higher tissue lactate levels[7], more troponin I release[8], higher levels of oxidative stress[9], and less available adenosine triphosphate (ATP)[10] compared to acyanotic myocardium. Moreover, cyanotic infants exhibit more myocardial injury during bypass surgery and worse postoperative outcomes[8,10]. Little is known about the mechanisms that contribute to the cyanotic myocardium's vulnerability to metabolic derangements during surgery.

The transition from the hypoxic fetal milieu to the oxygen-rich postnatal environment is thought to stimulate postnatal maturation[11]. Accordingly, a limited number of studies suggest that hypoxia delays cardiac maturation. In mice, postnatal hypoxia prolongs the neonatal period of cardiomyocyte proliferative ability[12]; and in chickens, prenatal hypoxia results in immature calcium handling[13]. Moreover, cardiomyocytes sampled from human patients with hypoplastic left heart syndrome show some persistence in fetal gene programming[14]. However, the direct

effects of chronic perinatal hypoxia on the developmental processes of the cardiomyocyte remain largely unknown.

To the best of our knowledge, this is the first study to examine the combined effects of pre- and postnatal hypoxia on the developing heart. The current study aimed to establish a rodent model of chronic perinatal hypoxia, as would be seen in cyanotic CHD, to investigate the developmental status of the cardiomyocyte under these conditions. We hypothesized that exposure to chronic hypoxia, beginning prenatally and continuing through the neonatal period, would perturb cardiomyocyte gene expression, contractile function, and the electrophysiologic substrate of the heart. The Cardiac Safety Research Consortium has implored the research community to perform more studies of developmental cardiac physiology to better understand the substrate on which therapies may work in the pediatric population[15], and this study intended to contribute to that call for knowledge.

Methods

Ethical Approval

Animal experiments were approved by the Institutional Animal Care and Use Committee at Children's National Research Institute, in compliance with the *NIH Guide for the Care and Use of Laboratory Animals*.

Animal Model

Wild-type pregnant CD1 mouse dams (6-8-week-old Crl:CD1(ICR) mice, Charles River Laboratories) were kept in a hypoxic chamber (BioSpherix, Redfield, NY) starting on embryonic day (E)16, a time that coincides with myocardial reliance on coronary flow for oxygen delivery and the beginning of a period of rapid growth of the ventricular myocardium, similar to the second trimester in human fetuses[16,17] (**Figure 1)**. During the experiment, the oxygen concentration was maintained, monitored, and recorded continuously with sensors placed inside

the chamber to achieve a level of 10.5 ± 0.5% (Pro:Ox Model 360, BioSpherix, Redfield, New York). Nitrogen gas was used to displace oxygen. Dams gave birth in the hypoxic chamber and pups remained in hypoxia until postnatal day (P)8, when cardiomyocyte maturation is nearly complete[18,19]. Strain and age-matched normoxic dams were kept in normoxia and gave birth under normoxic conditions. After P8, hypoxic animals were moved to normoxic conditions and allowed to recover until further testing at P30, thus simulating the return to normal oxygen saturations in human infants who have undergone definitive repair of cyanotic CHD.

Gene Expression

Whole hearts were excised and flash frozen in liquid nitrogen. Total RNA was isolated using an RNeasy fibrous tissue kit. Verification of RNA integrity and RNA quantification were done by spectrophotometry and an RNA 6000 Nano assay (Bioanalyzer 2100, Agilent Technologies). The RNA integrity number for all samples was >6 (mean=8.6 +/- SEM 0.19). Total RNA (250 ng) was primed for the entire length of RNA, including both poly(A) and non-poly(A) mRNA and reverse transcribed to generate sense-strand targets that were biotin-labelled using a WT Plus Reagent kit, and then hybridized to Affymetrix GeneChip Mouse Clariom S arrays for 16 hours (48°C), following manufacturer's instructions (Thermo Fisher Scientific). Hybridization cocktails were removed, and arrays were washed and stained on a Fluidics Station 450 (mouse Clariom S arrays). Arrays were scanned on the Affymetrix GCS3000 7G scanner and initial quality control data evaluated using Affymetrix Expression Console software (Thermo Fisher Scientific). Microarray data was imported and analyzed using the Transcriptome Analysis Console (Applied Biosciences). Gene ontology (GO) enrichment analysis was performed with the GOrilla tool using a single rank-ordered gene list[20,21]. The GOrilla *Mus musculus* GO database is updated frequently, and was last updated May 16, 2020 at the time of analysis.

In-Vivo Electrocardiography

Non-invasive electrocardiogram (ECG) recordings were obtained using an ecgTUNNEL system (emka Technologies). ECG waveforms were recorded for two minutes on P8 conscious and isoflurane-sedated animals as well as P30 conscious animals. ECG segments were quantified using ecgAuto software (emka Technologies) for heart rate, heart rate variability, atrial depolarization time (P-wave duration), atrioventricular conduction time (PR interval), ventricular depolarization time (QRS duration), and ventricular repolarization time (QT interval). Heart rate variability was measured as a root mean square of the successive differences (RMSSD)[22,23].

Ex-Vivo Electrophysiology Study

P30 animals were anesthetized with 4% isoflurane, the heart was rapidly excised and the aorta cannulated. The heart was transferred to a temperature-controlled (37°C) constant-pressure (70 mmHg) Langendorff perfusion system. Excised hearts were perfused with Krebs-Henseleit buffer bubbled with carbogen, as previously described[23,24]. A stimulation electrode was placed externally on the right atrium, and an atrial pacing protocol was used to determine Wenckebach cycle length (WBCL) and atrioventricular nodal effective refractory period (AVNERP). WBCL is the shortest pacing cycle length during atrial pacing that causes the Wenckebach phenomenon. AVNERP is the shortest extrastimulus interval during atrial pacing that fails to conduct through the atrioventricular (AV) node, as indicated by loss of ventricular capture. For ventricular pacing, a stimulation electrode was placed on the LV epicardium. To determine the ventricular effective refractory period (VERP), dynamic pacing was performed with stepwise decrements in the pacing cycle length (S1-S2) until loss of capture was noted. Baseline rhythms were monitored throughout the duration of the studies for detection of dysrhythmias including ectopy, sinus node dysfunction, and AV nodal block.

High Frequency Ultrasound Echocardiography

P30 animals underwent sedated transthoracic echocardiography to assess the persistent effects of chronic perinatal hypoxia on left ventricular systolic function. Anesthesia was initiated and maintained with inhaled isoflurane (1.5-2%). A pre-clinical high-frequency ultrasound system (VisualSonics Vevo 770, 30mHz probe) was used to obtain fractional shortening in a parasternal short axis view using M-mode measurements.

Statistical Analysis

Statistical analysis was performed using GraphPad Prism. Data normality was confirmed by Shapiro-Wilk test. Datasets were compared using two-sample Student's independent t-test or 2-way ANOVA with 0.1 false discovery rate to control for multiple comparisons testing (q value reported). Nonparametric datasets were compared using the Mann-Whitney test. Significance was defined as $p<0.05$.

Results

Hypoxia decreased litter size and pup weight

Hypoxic litters had markedly fewer pups than normoxic litters ($n\geq5$ litters per group, mean 5.7 vs 12.4 pups per litter, p=0.0005, **Figure 2A**). Intrauterine growth restriction is observed in human newborns with cyanotic CHD[25,26]. Similarly, we observed that our hypoxic animals were smaller than normoxic controls at P8 ($n\geq25$, mean 3.4 vs 6.5 g, $p<0.0001$, **Figure 2B-C**). Despite lower body weight, heart weight was preserved in hypoxia such that it did not differ from control (n=10, mean 46 vs 44 mg, p=0.58). As a result, heart-to-body-weight ratios were higher in hypoxic animals (n=10, mean 8.0 vs 15.4 mg/g, $p<0.0001$).

After P8, hypoxic animals recovered in normoxic conditions, thus simulating the return to normal oxygen saturations that occurs after definitive repair of cyanotic CHD. At P30, hypoxic animals had undergone catch-up growth such that their body weight was only slightly lower than normoxic controls ($n\geq14$, mean 20.0 vs 22.7 g, p=0.015, **Figure 2D**). Heart weight trended

toward slightly lower in hypoxic animals compared to control ($n \geq 9$, mean 119 vs 141 mg, $p=0.079$), such that heart-to-body-weight ratios were equivalent between the groups ($n \geq 9$, mean 6.4 vs 6.3 mg/g, $p=0.95$).

Hypoxia altered global gene expression at P8

Gene expression arrays were performed on whole heart samples isolated at P8 to assess the effects of hypoxia at the end of the neonatal period of rapid cardiomyocyte development, and again at P30 after hypoxic animals had recovered in normoxia. Principal component analysis demonstrated that experimental groups (normoxia versus hypoxia) were well-separated by their mRNA expression profiles at P8, but this separation was negligible at P30 (**Figure 3A**). Using a 1.5-fold expression cut-off and a 10% false discovery rate to correct for multiple testing[27], a total of 1427 mRNAs were differentially expressed between hypoxic and control hearts at P8 (**Figure 3B**; complete gene list in **Supplemental Table 1**). Differentially-expressed genes important to cardiac functioning and development are highlighted in the **Figure 3C** volcano plot. Within treatment groups, hypoxic animals exhibited a greater number of gene changes between P8 and P30 (4593 genes; **Figure 3B**) than the normoxic group (2147 genes), suggesting that the hypoxic group underwent more developmental changes over this time period after transitioning to normoxia. Interestingly, only one gene was expressed differentially between groups at P30: Wsb2 (WD repeat and SOCS box-containing 2).

Differentially expressed genes at P8 were significantly overrepresented in >400 GO categories (319 biological processes, 42 molecular functions, 46 cellular components**;** complete GO list in **Supplemental Table 2**). Categories associated with phenotypic changes observed in our experimental studies included extracellular matrix structural constituent (GO:0005201), ion channel binding (GO:0044325), glycolytic process (GO:0006096), hypoxia-inducible factor-1alpha signaling pathway (GO:0097411), mitotic cell cycle process (GO:1903047), and cell maturation (GO:0048469) (**Figure 4**).

Hypoxia altered transmembrane ion channel expression

Multiple transmembrane ion channels were differentially expressed in P8 hypoxic animals, including potassium (K^+), sodium (Na^+), and calcium (Ca^{++}) channels involved in the cardiac action potential and maintenance of a stable resting membrane (**Figure 5A**). In ventricular myocytes, phase 0 of the cardiac action potential is characterized by rapid depolarization via Na^+ influx (I_{Na}); voltage-gated Na^+ channel gene expression was upregulated with hypoxia (Scn3b: fold change +3.4, p=0.0002, q=0.017; Scn1b: fold change +1.3, p=0.018, q=0.15). Phase 1 is characterized by a fast transient outward K^+ current (I_{to}), which was downregulated in hypoxia (Kcnd2: fold change -8.02, p=0.0003, q=0.019; Kcnip2: fold change -3.17, p=0.0012, q=0.042; Kcnd3: fold change -1.46, p=0.0079, q=0.10). Notably, decreased I_{to} current is also observed in patients with atrial fibrillation[28] and heart failure[29], and can impair electromechanical coupling and prolong action potential duration[30]. Phase 1 also includes slow Na^{++} efflux via the Na^+/Ca^{++} exchanger (NCX1), which was upregulated in hypoxia (Slc8a1: fold change +2.78, p=0.0001, q=0.012). The plateau phase (phase 2) is primarily responsible for action potential duration. Membrane potential is held stable by balancing Ca^{++} influx and K^+ efflux, and both were affected by hypoxia. Ca^{++} influx continues via NCX1 (upregulated in hypoxia, see above), and L-type voltage-gated Ca^{++} channels open to increase Ca^{++} influx (I_{CaL}). I_{CaL} channels were downregulated in hypoxia (Cacna2d1: fold change -1.96, p=0.0014, q=0.045). Calmodulin expression was increased (Calm3: fold change +1.67, p=0.0009, q=0.036) which modulates both action potential duration and excitation-contraction coupling by modifying I_{CaL}. Slow K^+ efflux (I_{Ks}) occurs via voltage-gated K^+ channels, which were upregulated in hypoxia (Kcnq1: fold change +2.54, p=0.0057, q=0.089). Final rapid repolarization (phase 3) occurs mainly by K^+ efflux (I_{Kr}). Both genes associated with I_{Kr} trended toward downregulation (Kcne2: fold change -1.47, p=0.22, q=0.51; Kcnh2: fold change -1.24, p=0.28, q=0.57). Finally, phase 4 represents

the resting membrane potential which is maintained via constant K^+ efflux (I_{K1}, I_{Ach}, I_{ATP}) through inwardly rectifying K^+ channels; these genes were largely unaffected by hypoxia.

In cardiac pacemaker cells, the T-type Ca^{++} channel generates Ca^{++} influx (I_{CaT}) to initiate an action potential (gene = Cacna1g). Cacna1g had a 3.13 fold down-regulation which did not meet significance (p=0.052, q=0.26). Additional studies are needed to examine regional differences in T-type Ca^{++} channel expression, which can result in bradycardia and sinus node dysfunction if localized to pacemaker cells. Finally, gap junctions connect neighboring cardiomyocytes and allow for rapid spread of an action potential from one cell to the next. Gap junction expression was downregulated in hypoxia (Gja1: fold change -2.57, p=0.0022, q=0.056; Gja6: fold change -1.74, p=0.0067, q=0.096), which can lead to slower electrical conduction.

Hypoxia altered expression of genes important to the contractile apparatus

Multiple genes important to the contractile apparatus were differentially expressed in P8 hypoxic animals, including those involved in both calcium handling and sarcomere structure (**Figure 5B**). Within the cardiac sarcomere, isoform switching occurs during perinatal development for many key structural proteins. In hypoxic P8 animals, there was persistence of immature isoforms of Troponin-I (Tnni1: fold change +13.13, p=9.71E-05, q=0.011), alpha-actin (Acta1: fold change +5.57, p=0.012, q=0.12), gamma-actin (Actg1: fold-change +3.05, p=0.010, q=0.12), and myosin heavy chain (Myh7: fold change +1.48, p=0.083, q=0.32); although only Troponin-I met the predetermined threshold for significance. The isoform switch for myosin light chain was unaffected (Myl7→Myl2), however expression of two myosin light chain regulators were altered (Myl3: fold change -1.79, p=0.0045, q=0.08; Myl9: fold change +5.48, p=0.0025, q=0.06).

Multiple stabilizing components of the cardiac sarcomere were also altered in P8 hypoxic animals. Titin, the cardiac myofilament responsible for passive tension, was downregulated in

hypoxia (fold change -2.56, p=0.0055, q=0.088), which may cause an increased risk for diastolic dysfunction[31]. Desmin provides strength of attachment of myofibrils to the Z-disk, and was upregulated in hypoxia (Des: fold change +2.31, p=0.0023, q=0.057). Desmosomes and adherens junctions provide structural integrity between cells, and both demonstrated downregulation of components in hypoxia (Pkp1: fold change -1.55, p=0.0022, q=0.056; Pcdh7: fold change -1.82, p=0.0025, q=0.061; Dsc2: fold change -2.04, p=0.016, q=0.14). Vimentin expression was increased (Vim: fold change +3.08, p=0.0017, q=0.050) indicating an increased fibroblast population, but collagen expression was decreased (extracellular matrix cluster in **Figure 4B**), suggesting decreased fibroblast functioning and a less robust extracellular matrix to act as a scaffold for muscle contraction.

Calcium handling genes were also altered in hypoxic P8 animals. In mature cardiomyocytes, synchronized ryanodine receptors facilitate a rapid increase in cytosolic Ca^{++} concentration which is necessary for excitation-contraction coupling. Ryanodine receptor expression was decreased in hypoxic animals (Ryr2: fold change -3.74, p=0.0038, q=0.073; Ryr1: fold change -1.16, p=0.029, q=0.20), consistent with a delay in maturation. Further, extracellular Ca^{++} entry may be altered in hypoxic animals due to decreased expression of L-type calcium channels (Cacna2d1, see above) and increased expression of the Na^{+}/Ca^{++} exchanger (Slc8a1, see above). The sarco-endoplasmic reticulum Ca^{++}-ATPase (SERCA) pumps calcium from the cytoplasm back into the sarcoplasmic reticulum in preparation for the next cardiac cycle. Hypoxia decreased SERCA expression (Atp2a3: fold change -2.03, p=0.0005, q=0.027), which could decrease sarcoplasmic reticulum Ca^{++} load, reduce contractility, and slow lusitropy.

Hypoxia caused bradycardia, slowed conduction velocity, and isoflurane effects at P8

With the observed changes in ion channel expression on gene arrays, we collected *in-vivo* ECG tracings at P8 (**Figure 6A**) to identify alterations in the electrophysiologic substrate of the heart immediately after chronic perinatal hypoxia. During normal murine development, heart rate

increases as maturation progresses. At P8, hypoxic animals were bradycardic compared to normoxic controls ($n \geq 10$, mean 308 vs 543 beats per minute, $p<0.0001$), consistent with a delay in normal postnatal maturation (**Figure 6B**). We examined the effects of isoflurane sedation on ECG measurements, as cyanotic newborns with CHD are subjected to anesthesia at the time of surgical repair. Isoflurane sedation had a bradycardic effect in both groups; however, the hypoxic animals remained more bradycardic than normoxic when sedated ($n \geq 10$, mean 204 vs 272 beats per minute, $q=0.0020$, **Figure 6C**).

Conduction speed is expected to increase throughout development as cell-cell interactions mature. P8 hypoxic animals had a longer P-wave duration ($n \geq 7$, mean 15.0 vs 12.2 msec, $p=0.017$), PR interval ($n \geq 8$, mean 53.0 vs 37.5 msec, $p<0.0001$), QRS duration ($n \geq 10$, mean 15.5 vs 13.3 msec, $p=0.012$), and QT interval ($n \geq 10$, mean 61.3 vs 38.8 msec, $p<0.0001$) compared to normoxic controls (**Figure 6B**). QT intervals were analyzed in sedated animals, as this parameter could not be measured accurately in active P8 animals. Isoflurane sedation prolonged PR interval in both groups, but the effect was more dramatic in hypoxic animals ($n \geq 8$, interaction $p=0.031$, $F=5.03$, **Figure 6C**). Anesthetic agents have been reported to slow atrioventricular conduction in animal models[32,33] and human case reports[34,35], and our results suggest that perinatal hypoxia exaggerates this effect. We also observed a significantly lower heart rate variability in sedated hypoxic animals compared with normoxic controls ($n \geq 10$, median 1.7 vs 3.4 msec, $q=0.0009$, **Figure 6C**). Importantly, heart rate variability increases with age during normal development[23].

ECG measurements normalized at P30 after a period of recovery in normoxia

Since genetic differences had resolved at P30 after recovering in normoxia, ECG measurements were repeated at P30 to determine if electrophysiologic differences had also normalized. At P30, there was no difference in heart rate ($n \geq 4$, mean 407 vs 406 beats per minute, $p=0.98$), heart rate variability ($n=4$, median 13.6 vs 8.0 msec, $q=0.34$), or QRS duration

(n≥4, mean 15.1 vs 15.3 msec, p=0.84) between groups (**Figure 6B**). Hypoxic animals still had a trend toward longer P-wave duration (n≥4, mean 19.3 vs 16.1 msec, p=0.24), PR interval (n≥4, mean 44.4 vs 38.9 milliseconds, p=0.39), and QT interval (n≥4, mean 23.9 vs 21.9 msec, p=0.29) (**Figure 6B**). The significant differences in ECG parameters observed at P8 largely abated after the 22 day period of recovery in normoxia, consistent with gene expression data (**Figure 3A-B)**.

Ex-vivo electrophysiology study revealed persistent underlying changes to the electrophysiologic substrate after hypoxia

Although ECG measurements largely normalized by P30, we conducted more rigorous testing of the cardiac electrophysiologic substrate in the absence of autonomic influences. Electrophysiology studies performed at P30 revealed that perinatal hypoxia caused persistent prolongation of VERP compared to normoxic controls (n=4, mean 76.5 vs 46.5 msec, p=0.013), a parameter that normally decreases with age (**Figure 7A**). No difference in atrioventricular conduction was observed between groups, measured by WBCL (n=4, mean 84.0 vs 84.5 msec, p=0.94) and AVNERP (n=4, mean 72.8 vs 70.5 msec, p=0.76) (**Figure 7A**). *Ex-vivo* studies also revealed sinus node dysfunction in 100% of the hypoxic hearts, as opposed to 25% of the normoxic control hearts (**Figure 7B,C**). Cyanotic CHD carries a high incidence of sinus node dysfunction[36,37], and our results suggest that hypoxia may play a role in creating the substrate for sinus node dysfunction.

Perinatal hypoxia caused a persistent decrease in contractile function

Gene expression changes indicated differences in the sarcomere and calcium handling at P8, and we sought to measure phenotypic contractile function after recovery in normoxia. Transthoracic echocardiography at P30 demonstrated decreased fractional shortening in

319 animals exposed to hypoxia as compared to normoxic controls ($n \geq 3$, mean 0.29 vs 0.38,
320 p=0.027, **Figure 8**), consistent with worse contractile function.

321 ## Discussion

322 Our results support our hypothesis that cardiac maturation is perturbed in a mouse model of
323 chronic perinatal hypoxia. Chronic perinatal hypoxia altered both the electrophysiologic
324 substrate and the contractile apparatus. Although the majority of differences detected at P8
325 normalized after recovering in normoxia, there were persistent alterations at P30 that may
326 contribute to lifelong mortality and morbidity in the cyanotic CHD population.

327 Numerous genetic and phenotypic differences were detected at P8. Hypoxia altered global gene
328 expression and ECG parameters, including bradycardia, slowed conduction speed, and
329 decreased heart rate variability and exaggerated PR prolongation with sedation. In our animal
330 model, P8 represents the time of surgical repair, and therefore, phenotypic differences in
331 hypoxic animals may have implications for surgical outcomes and the immediate post-surgical
332 course. Disturbances in ion channel expression may explain ECG disturbances at P8, and may
333 predispose the hypoxic heart to arrhythmias. Specifically, reduced I_{to} current and an altered
334 plateau phase can prolong the action potential, and reduced gap junctions can slow electrical
335 conduction across the heart. Likewise, decreases in extracellular matrix collagen and alterations
336 in the contractile apparatus have the potential to affect the strength of cardiac contraction.
337 Electromechanical coupling development was especially delayed in hypoxic animals, as
338 demonstrated by decreased L-type Ca^{++} channel, ryanodine receptor, and SERCA pump
339 expression; all of which can contribute to a blunted increase in cytosolic Ca^{++} concentration and
340 therefore weaker contraction. Increased dependence on glycolysis (**Figure 4**) may reduce
341 myocardial energy reserves, as observed in infants undergoing surgical repair[6–10]. Furthermore,
342 if myocardial growth continues by cell proliferation instead of hypertrophy, there is an increased
343 risk of cell structure abnormalities. Notably, some differentially expressed genes in our study are

associated with clinical sudden arrhythmic death syndromes[38] (long QT syndrome, Brugada syndrome, arrhythmogenic right ventricular dysplasia, catecholaminergic polymorphic ventricular tachycardia) and clinical cardiomyopathies[39] (dilated, hypertrophic, left ventricular noncompaction).

In our model, P30 represents recovery after early definitive repair of cyanotic CHD. Gene expression and ECG differences observed at P8 largely resolved by P30, suggesting that the heart was able to complete development after a return to normal oxygen conditions. This is an optimistic sign that many of the observed effects from chronic perinatal hypoxia may be reversible with early repair. However, *ex-vivo* electrophysiology studies revealed persistent changes to the underlying electrophysiologic substrate including prolonged VERP and increased sinus node dysfunction, and echocardiogram revealed persistent decreased contractile function. This is similar to previous animal studies of pre- or postnatal hypoxia, which demonstrated both systolic and diastolic dysfunction[13,40–42]; however, this is the first study demonstrating persistent electrophysiologic changes after perinatal hypoxia. Importantly, measurements of gene expression do not necessarily reflect differences in protein expression and localization, ion channel current, or the myofilament and sarcomere architecture. Studies suggest that prenatal hypoxia imprints on a fetus and causes lifelong changes to the cardiovascular system, such as increased susceptibility to systemic hypertension and metabolic syndrome and worse response to myocardial infarction[43]. Further investigation is required to define proteomic, metabolic, and ion current changes that persist after recovery from chronic perinatal hypoxia.

To date, there has been limited investigation into the effects of hypoxia on the developing heart, and thus there is no established animal model. The main embryological progression of heart development is the same between humans and rodents[44]. The early embryonic heart is thin-walled and relies on diffusion of oxygen from the chambers until the coronaries connect to the

aorta[44], at which point the myocardium starts to grow and thicken[18,44]. This timeline was the rationale for starting hypoxia on embryonic day 16, when the coronary development is complete[17,45]. This timing captures the period of rapid ventricular growth that occurs in both species once the myocardium is reliant on the coronary circulation for oxygen delivery. For both humans and rodents, there are similar changes in myocyte proteins for the remainder of gestation, and both demonstrate rapid and marked development in the first postnatal week, reaching definitive adult cell function and morphology quickly after the postnatal change in loading conditions and oxygenation[18,19].

Our study aimed to be a proof of concept, that chronic perinatal hypoxia disrupts the process of normal cardiac development. To our knowledge, this is the first study to include both pre- and postnatal hypoxia to model the range of cardiac development affected by hypoxia in cyanotic CHD. Further, we incorporated a period of recovery to simulate definitive repair of cyanotic CHD. Toward this goal, our mice displayed characteristics consistent with human cyanosis, such as lower birth weight[25,26], and replicated increased heart-to-body-weight ratios reported in previous hypoxia animal studies[46,47]. Limitations of our model include the inherent constraints of using small animals to model human disease, and the risk of introducing maternal stress into gestation[48,49]. Litter size was reduced in our animals, which may be evidence for maternal stress. Importantly, the comparative effect of degree of hypoxia between species is unknown. We chose 10.5% for the degree of hypoxia, as a fractional inspired oxygen concentration (FiO_2) of 10% correlates with pulse oximetry readings of 55-70% in rodents[50]. For comparison, human fetuses with cyanotic CHD have a mean oxygen saturation of 48% in the ascending aorta[5], and neonates have target oxygen saturation ranges of 70-85%. Despite the unknowns between species, we believe this study is a first step toward understanding the impact of hypoxia on cardiac development.

The Cardiac Safety Research Consortium has implored the research community to perform more studies of developmental cardiac physiology to better understand the substrate on which cardiac therapies may work in the pediatric population[15]. Further studies regarding the effects of hypoxia on cardiac development may allow us to better target cardiac therapeutics for the cyanotic CHD population. A better understanding of the effects of chronic perinatal hypoxia on cardiac development could lead to improved surgical outcomes and overall improved cardiovascular health in the cyanotic CHD population.

400 **Acknowledgments:** We gratefully acknowledge Dr. Susan Knoblach, Karuna Panchapakesan,
401 and the Children's National Research Institute Genomics and Bioinformatics Core for assistance
402 with microarray experiments; we also acknowledge Dr. Norman Lee for assistance with
403 heatmap analysis, and Drs. Christopher Spurney and Charles Berul for helpful discussions.

404 **Sources of Funding:** This work was supported by the NIH (R01HL139472 to NGP,
405 R01HL139712 and R01HL146670 to NI), Children's National Heart Institute, and the Office of
406 the Assistant Secretary of Defense for Health Affairs through the Peer Reviewed Medical
407 Research Program under Award No. W81XWH2010199 (N.I.). This publication was also
408 supported by the Gloria and Steven Seelig family.

409 **Disclosures:** None.

410 **Author Contributions:** JR, ZD, CM, DG, MR, LS, NV, MR performed experiments; JR, ZD,
411 CM, NGP analyzed data; JR, DG, NGP prepared figures; JR, NGP drafted manuscript; JR, ZD,
412 NI, NGP conceived and designed experiments; all authors approved manuscript.

References

1. Reller MD, Strickland MJ, Riehle-Colarusso T, Mahle WT, Correa A. Prevalence of Congenital Heart Defects in Metropolitan Atlanta, 1998-2005. *J Pediatr*. 2008;153:807–813.

2. Oster ME, Lee KA, Honein MA, Riehle-Colarusso T, Correa A. Temporal Trends in Survival Among Infants With Critical Congenital Heart Defects HHS Public Access. *Pediatrics*. 2013;131:1502–1508.

3. Hinton RB, Ware SM. Heart Failure in Pediatric Patients with Congenital Heart Disease. *Circ Res*. 2017;120:978–994.

4. Dinardo JA. Heart failure associated with adult congenital heart disease. *Semin Cardiothorac Vasc Anesth*. 2013;17:44–54.

5. Sun L, Macgowan CK, Sled JG, Yoo S-J, Manlhiot C, Porayette P, Grosse-Wortmann L, Jaeggi E, McCrindle BW, Kingdom J, Hickey E, Miller S, Seed M. Reduced Fetal Cerebral Oxygen Consumption is Associated With Smaller Brain Size in Fetuses With Congenital Heart Disease. *Circulation*. 2015;131:1313–1323.

6. Teoh KH, Mickle DA, Weisel RD, Li RK, Tumiati LC, Coles JG, Williams WG. Effect of oxygen tension and cardiovascular operations on the myocardial antioxidant enzyme activities in patients with tetralogy of Fallot and aorta-coronary bypass. *J Thorac Cardiovasc Surg*. 1992;104:159–64.

7. Modi P, Suleiman MS, Reeves BC, Pawade A, Parry AJ, Angelini GD, Caputo M. Basal metabolic state of hearts of patients with congenital heart disease: The effects of cyanosis, age, and pathology. *Ann Thorac Surg*. 2004;78:1710–1716.

435 8. Imura H, Caputo M, Parry A, Pawade A, Angelini G, Suleiman M. Age-Dependent and
436 Hypoxia-Related Differences in Myocardial Protection During Pediatric Open Heart
437 Surgery Improved Surgical Outcome After Fetal Diagnosis of Hypoplastic Left Heart
438 Syndrome. *Circulation*. 2001;103:1551–1556.

439 9. Ercan S, Cakmak A, Kösecik M, Erel O. The oxidative state of children with cyanotic and
440 acyanotic congenital heart disease. *Anadolu Kardiyol Derg*. 2009;9:486–90.

441 10. Najm HK, Wallen WJ, Belanger MP, Williams WG, Coles JG, Arsdell GS Van, Black MD,
442 Boutin C, Wittnich C. Does the degree of cyanosis affect myocardial adenosine
443 triphosphate levels and function in children undergoing surgical procedures for congenital
444 heart disease? *J Thorac Cardiovasc Surg*. 2000;119:515–524.

445 11. Patterson AJ, Zhang L. Hypoxia and fetal heart development. *Curr Mol Med*.
446 2010;10:653–66.

447 12. Puente BN, Kimura W, Muralidhar SA, Moon J, Amatruda JF, Phelps KL, Grinsfelder D,
448 Rothermel BA, Chen R, Garcia JA, Santos CX, Thet S, Mori E, Kinter MT, Rindler PM,
449 Zacchigna S, Mukherjee S, Chen DJ, Mahmoud AI, Giacca M, Rabinovitch PS,
450 Aroumougame A, Shah AM, Szweda LI, Sadek HA. The oxygen-rich postnatal
451 environment induces cardiomyocyte cell-cycle arrest through DNA damage response.
452 *Cell*. 2014;157:565–579.

453 13. Jonker SS, Giraud GD, Espinoza HM, Davis EN, Crossley DA. Effects of chronic hypoxia
454 on cardiac function measured by pressure-volume catheter in fetal chickens. *Am J*
455 *Physiol Integr Comp Physiol*. 2015;308:R680–R689.

456 14. Bohlmeyer TJ, Helmke S, Ge S, Lynch J, Brodsky G, Sederberg JH, Robertson AD,
457 Minobe W, Bristow MR, Perryman MB. Hypoplastic left heart syndrome myocytes are

differentiated but possess a unique phenotype. *Cardiovasc Pathol*. 2003;12:23–31.

15. Bates KE, Vetter VL, Li JS, Cummins S, Aguel F, Almond C, Dubin AM, Elia J, Finkle J, Hausner EA, Joseph F, Karkowsky AM, Killeen M, Lemacks J, Mathis L, McMahon AW, Pinnow E, Rodriguez I, Stockbridge NL, Stockwell M, Tassinari M, Krucoff MW, Providence U. Pediatric cardiovascular safety: Challenges in drug and device development and clinical application. *Am Heart J*. 2012;164:481–492.

16. Olivey HE, Compton LA, Barnett J V. Coronary Vessel Development The Epicardium Delivers. *Trends Cardiovasc Med*. 2004;14:247–251.

17. Theveniau-Ruissy M, Perez-Pomares J-M, Parisot P, Baldini A, Miquerol L, Kelly RG. Coronary stem development in wild-type and Tbx1 null mouse hearts. *Dev Dyn*. 2016;245:445–459.

18. Porter GA, Hom JR, Hoffman DL, Quintanilla RA, Bentley KL d. M, Sheu SS. Bioenergetics, mitochondria, and cardiac myocyte differentiation. *Prog Pediatr Cardiol*. 2011;31:75–81.

19. Scuderi GJ, Butcher J. Naturally Engineered Maturation of Cardiomyocytes. *Front Cell Dev Biol*. 2017;5:1–28.

20. Eden E, Navon R, Steinfeld I, Lipson D, Yakhini Z. GOrilla: A Tool For Discovery And Visualization of Enriched GO Terms in Ranked Gene Lists. *BMC Bioinformatics*. 2009;10:48.

21. Eden E, Lipson D, Yogev S, Yakhini Z. Discovering Motifs in Ranked Lists of DNA sequences. *PLoS Comput Biol*. 2007;3:e39.

22. Task Force of the European Society of Electrophysiology. Heart Rate Variability:

480 Standards of Measurement, Physiological Interpretation, and Clinical Use. *Circulation*.
481 1996;93:1043–1065.

482 23. Swift LM, Burke M, Guerrelli D, Reilly M, Ramadan M, McCullough D, Prudencio T,
483 Mulvany C, Chaluvadi A, Jaimes R, Posnack NG. Age-dependent changes in
484 electrophysiology and calcium handling: implications for pediatric cardiac research. *Am J*
485 *Physiol Circ Physiol*. 2020;318:H354–H365.

486 24. Jaimes R, McCullough D, Siegel B, Swift L, McInerney D, Hiebert J, Perez-Alday E,
487 Trenor B, Sheng J, Saiz J, Tereshchenko L, Posnack N. Plasticizer Interaction With the
488 Heart: Chemicals Used in Plastic Medical Devices Can Interfere With Cardiac
489 Electrophysiology. *Circ Arrhythm Electrophysiol*. 2019;12:e007294.

490 25. Malik S, Cleves MA, Zhao W, Correa A, Hobbs CA. Association Between Congenital
491 Heart Defects and Small for Gestational Age. *Pediatrics*. 2007;119:e976-982.

492 26. Khoury MJ, Erickson JD, Cordero F, Mccarthy BJ. Congenital Malformations and
493 Intrauterine G rowth Retardation : A Population Study. *Pediatrics*. 1988;82:83–90.

494 27. Posnack NG, Lee NH, Brown R, Sarvazyan N. Gene expression profiling of DEHP-
495 treated cardiomyocytes reveals potential causes of phthalate arrhythmogenicity.
496 *Toxicology*. 2011;279:54–64.

497 28. Brandt MC, Priebe L, Böhle T, Südkamp M, Beuckelmann DJ. The ultrarapid and the
498 transient outward K+ current in human atrial fibrillation. Their possible role in
499 postoperative atrial fibrillation. *J Mol Cell Cardiol*. 2000;32:1885–1896.

500 29. Beuckelmann DJ, Näbauer M, Erdmann E. Alterations of K+ currents in isolated human
501 ventricular myocytes from patients with terminal heart failure. *Circ Res*. 1993;73:379–385.

30. Niwa N, Nerbonne JM. Molecular determinants of cardiac transient outward potassium current (Ito) expression and regulation. *J Mol Cell Cardiol*. 2010;48:12–25.

31. Lewinter MM, Granzier H. Cardiac Titin-A Multifunctional Giant. *Circulation*. 2010;121:2137–2145.

32. Kato K, Wakai J, Ozawa K, Sekiguchi M, Katahira K. Different sensitivity to the suppressive effects of isoflurane anesthesia on cardiorespiratory function in SHR/Izm, WKY/Izm, and Crl:CD (SD) rats. *Exp Anim*. 2016;65:393–402.

33. Raatikainen PMJ, Morey TE, Druzgala P, Milner P, Gonzalez MD, Dennis DM. Effects of Volatile Anesthetics on Atrial and AV Nodal Electrophysiological Properties in Guinea Pig Isolated Perfused Heart. *Anesthesiology*. 1998;89:434–442.

34. Mamiya K, Aono J, Manabe M. Complete atrioventricular block during anesthesia. *Can J Anaesth*. 1999;46:265–267.

35. Kamatani T, Akizuki A, Kondo S, Shirota T. Second-Degree Atrioventricular Block Occurring After Tooth Extraction. *Anesth Prog*. 2016;63:156–159.

36. Carlson SK, Patel AR, Chang PM. Bradyarrhythmias in Congenital Heart Disease. doi:10.1016/j.ccep.2017.02.002.

37. Triedman JK. Arrhythmias in adults with congenital heart disease. *Heart*. 2002;87:383–389.

38. Fulgent. Comprehensive Arrhythmia NGS Panel | Fulgent Genetics. Available at https://www.fulgentgenetics.com/comprehensive-arrhythmia. Accessed May 14, 2020.

39. Fulgent. Comprehensive Cardiomyopathy NGS Panel | Fulgent Genetics. Available at https://www.fulgentgenetics.com/comprehensive-cardiomyopathy. Accessed May 14,

2020.

40. Thompson LP, Chen L, Polster BM, Pinkas G, Song H. Prenatal hypoxia impairs cardiac mitochondrial and ventricular function in guinea pig offspring in a sex-related manner. *Am J Physiol Regul Integr Comp Physiol*. 2018;315:R1232–R1241.

41. Lindgren I, Altimiras J. Prenatal hypoxia programs changes in-adrenergic signaling and postnatal cardiac contractile dysfunction. *Am J Physiol Regul Integr Comp Physiol*. 2013;305:1093–1101.

42. Corno AF, Giuseppina Milano F, Samaja M, Tozzi P, von Segesser LK. Chronic hypoxia: A model for cyanotic congenital heart defects Corno et al Surgery for Congenital Heart Disease. *J Thorac Cardiovasc Surg*. 2002;124:105.

43. Giussani DA, Davidge ST. Developmental programming of cardiovascular disease by prenatal hypoxia. *J Dev Orig Health Dis*. 2013;4:328–337.

44. Wessels A, Sedmera D. Developmental anatomy of the heart: A tale of mice and man. *Physiol Genomics*. 2003;15:165–176.

45. Savolainen SM, Foley JF, Elmore SA. Histology atlas of the developing mouse heart with emphasis on E11.5 to E18.5. *Toxicol Pathol*. 2009;37:395–414.

46. Camm EJ, Hansell JA, Kane AD, Herrera EA, Lewis C, Wong S, Morrell NW, Giussani DA. Partial contributions of developmental hypoxia and undernutrition to prenatal alterations in somatic growth and cardiovascular structure and function. *Am J Obstet Gynecol*. 2010;203:495.e24-495.e34.

47. Corno AF, Milano G, Samaja M, Tozzi P, von Segesser LK. Chronic hypoxia: A model for cyanotic congenital heart defects. *J Thorac Cardiovasc Surg*. 2002;124:105–112.

546 48. Steurer MA, Peyvandi S, Baer RJ, Oltman SP, Chambers CD, Norton ME, Ryckman KK,
547 Moon-Grady AJ, Keller RL, Shiboski SC, Jelliffe-Pawlowski LL. Impaired Fetal
548 Environment and Gestational Age: What Is Driving Mortality in Neonates With Critical
549 Congenital Heart Disease? *J Am Heart Assoc*. 2019;8. doi:10.1161/JAHA.119.013194.

550 49. Gaynor JW, Parry S, Moldenhauer JS, Simmons RA, Rychik J, Ittenbach RF, Russell
551 WW, Zullo E, Ward JL, Nicolson SC, Spray TL, Johnson MP. The impact of the maternal-
552 foetal environment on outcomes of surgery for congenital heart disease in neonates. *Eur*
553 *J Cardiothorac Surg*. 2018;54:348–353.

554 50. Morgan BJ, Adrian R, Bates ML, Dopp JM, Dempsey JA. Quantifying hypoxia-induced
555 chemoreceptor sensitivity in the awake rodent. *J Appl Physiol*. 2014;117:816–824.

556 **Figures with Figure Legends:**

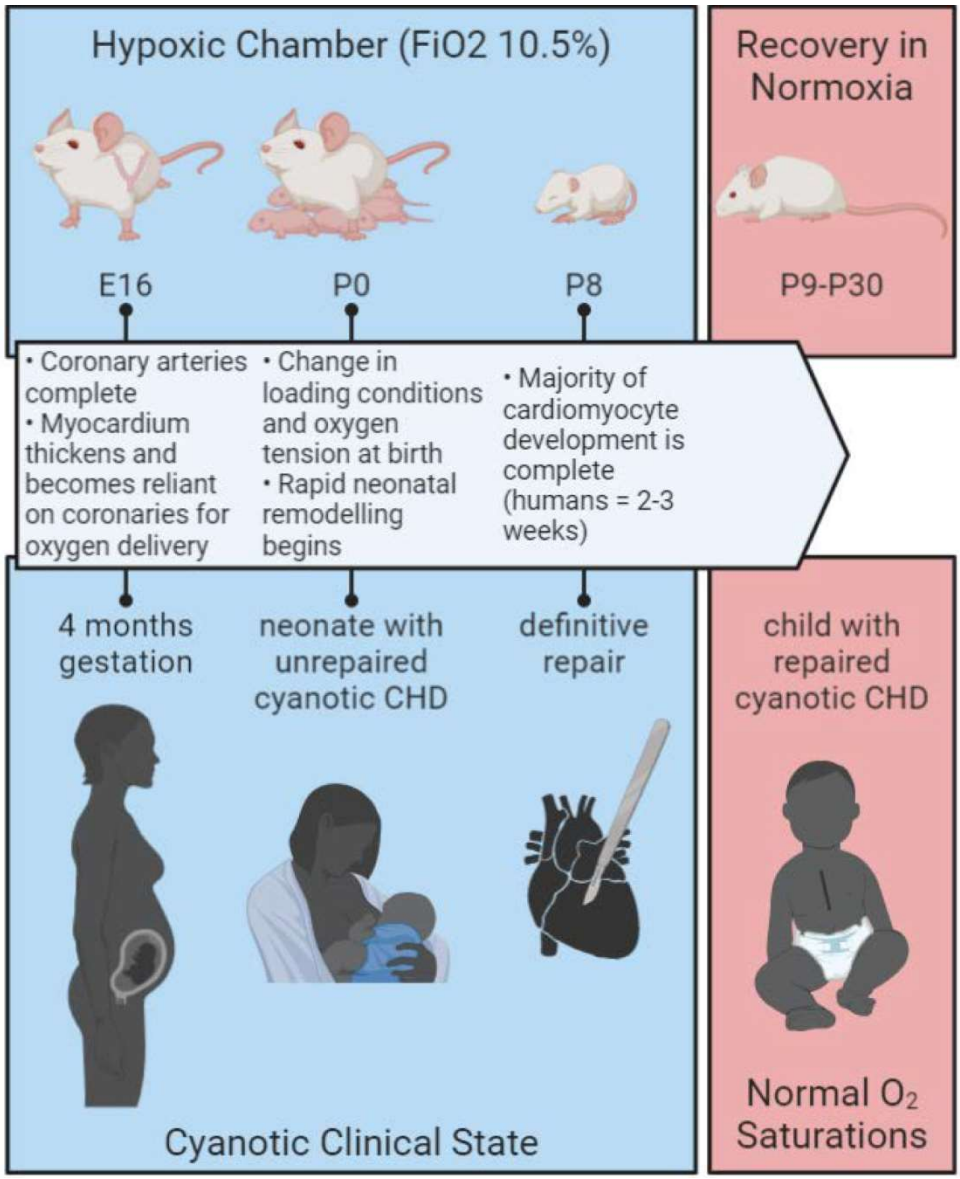

557

558 **Figure 1: Chronic Perinatal Hypoxia Mouse Model.** Pregnant CD1 mice were placed in
559 hypoxia starting on embryonic day (E)16, corresponding with rapid growth of the ventricular
560 myocardium and reliance on coronary arteries, similar to a 4 months gestation human fetus.
561 Hypoxic pups were born and reared in hypoxia until postnatal day (P)8 when the majority of
562 cardiomyocyte development is complete. Removal from the hypoxic chamber represents

563 definitive repair in human neonates with cyanotic CHD. Mice recovered in normoxia until further
564 testing at P30, representing a child with repaired cyanotic CHD and corresponding
565 normalization in oxygen saturations. FiO2, fractional inspired oxygen concentration. Image
566 created with Biorender.com.

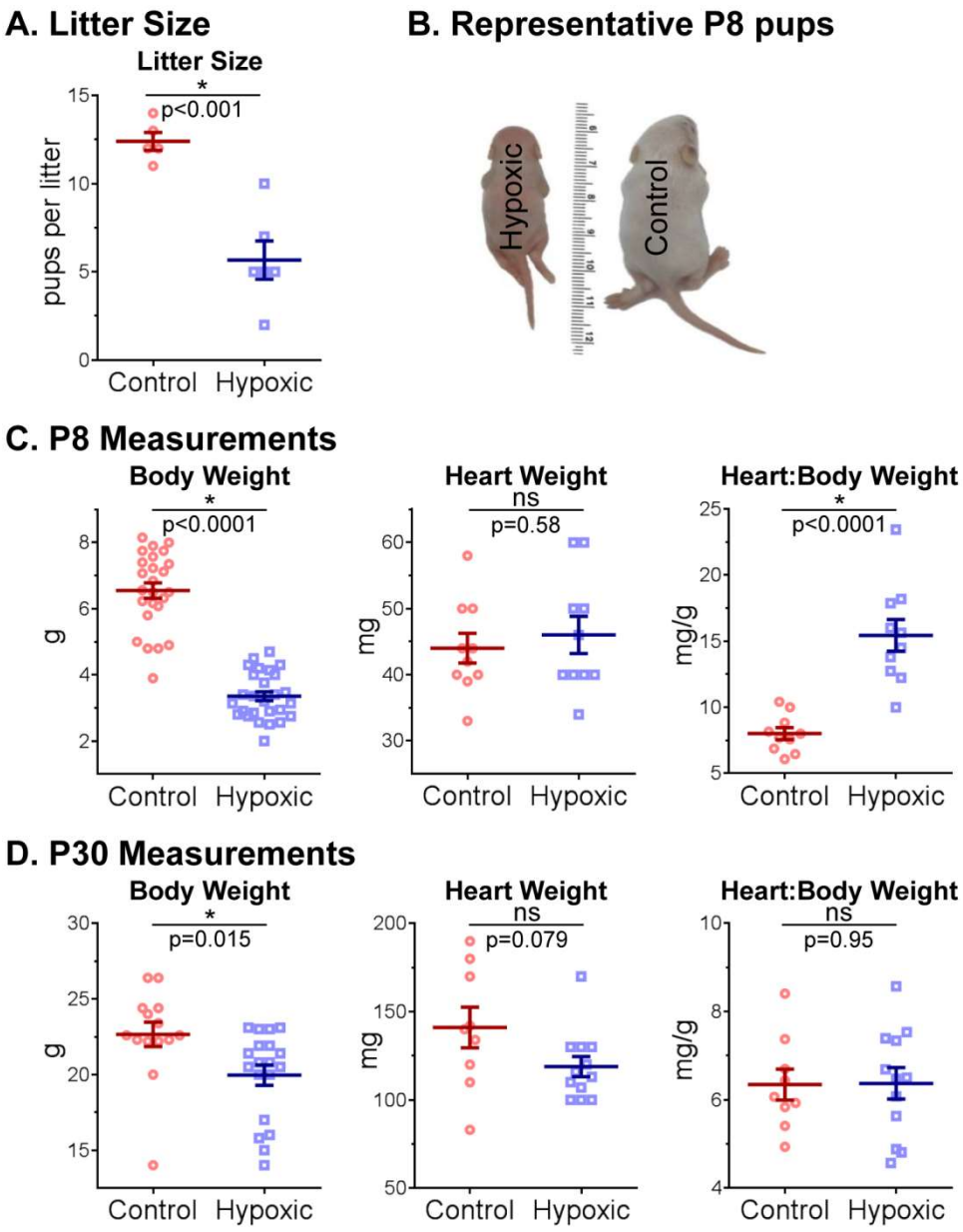

Figure 2: Litter Size and Body Measurements. A: Hypoxia reduced mean litter size. **B, C**: At P8, hypoxic animals were markedly smaller than control; however, heart weight was preserved, and thus heart-to-body-weight ratio was higher in hypoxic animals. **D:** By P30, hypoxic animals underwent catch-up growth such that they were only slightly smaller than control; heart weight trended toward slightly lower in hypoxic animals, and heart-to-body weight ratios were equivalent between groups. All data presented as mean ± SEM. *p<0.05, ns=not significant.

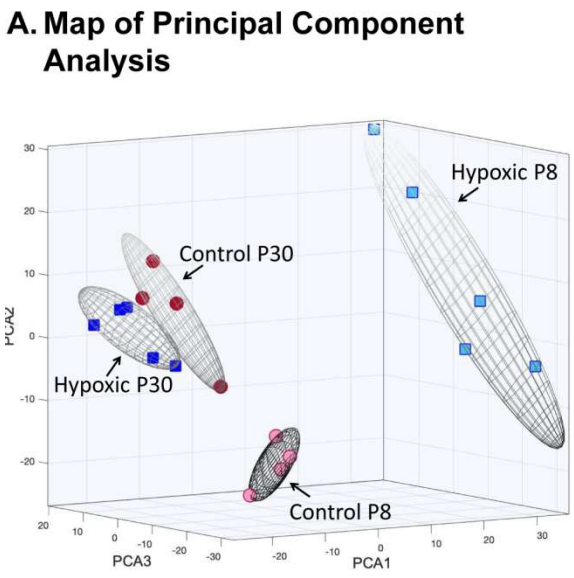

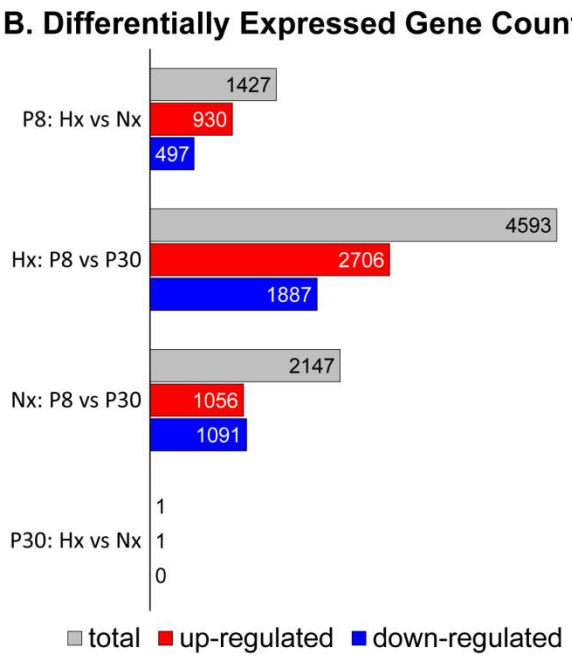

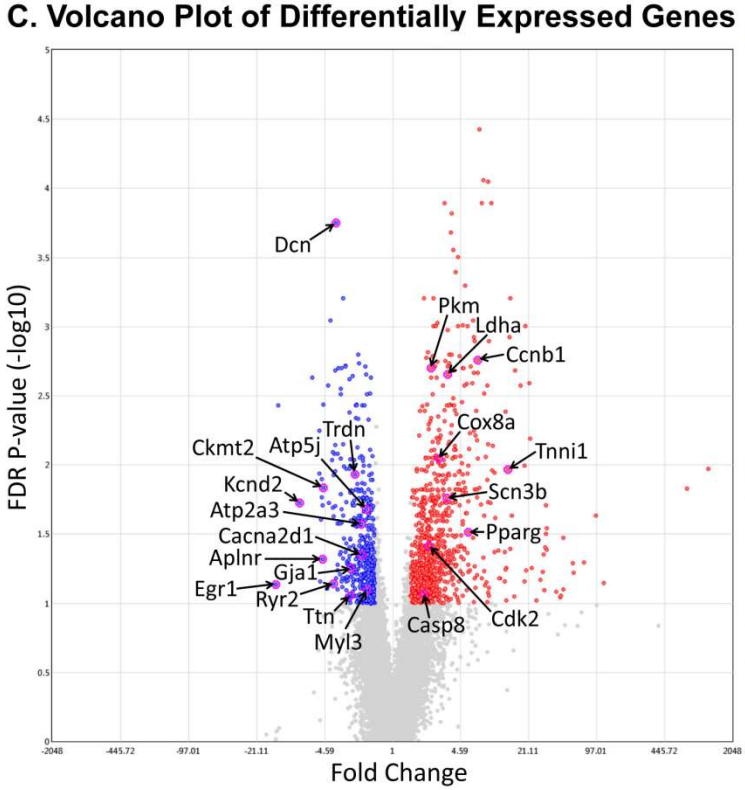

Gene	Function
Dcn	Collagen fibril assembly
Trdn	Excitation-contraction coupling
Ckmt2	Mitochondrial function
Kcnd2	Voltage-gated K+ channel
Atp5j	Oxidative phosphorylation
Atp2a3	SERCA pump
Cacna2d1	L-type Ca++ channel
Aplnr	Endogenous inotropy
Gja1	Gap junction/cell-cell interaction
Egr1	Transcriptional regulator
Ryr2	Excitation-contraction coupling
Myl3	Contractile strength
Ttn	Sarcomere structure

Gene	Function
Ccnb1	Cell cycle (G2/M transition)
Pkm	Glycolysis
Ldha	Anaerobic glycolysis
Cox8a	Oxidative phosphorylation
Tnni1	Immature contractile isoform
Scn3b	Voltage-gated Na+ channel
Pparg	Transcriptional regulator
Cdk2	Cell cycle (G1/S transition)
Casp8	Apoptosis/Necroptosis

Figure 3: Global Gene Expression. A: Principal component analysis demonstrated that experimental groups were well separated by their mRNA expression profiles at P8, but this separation was negligible in P30 samples. **B:** Using a 1.5-fold expression cut-off with 0.1 false-

discovery rate, a total of 1427 mRNAs were differentially expressed between hypoxic (Hx) and normoxic control (Nx) hearts at P8, with near resolution of differences by P30. **C:** Specific genes important to cardiovascular functioning and development are highlighted in a volcano plot of all differentially expressed genes between groups at P8.

A. Gene Ontologies

Key Downregulated GOs	p	FDR q	Enrichment
Extracellular matrix structural constituent	5.42E-6	2.42E-3	5.08
Ion channel binding	2.52E-4	3.34E-2	2.90
Key Upregulated GOs	**p**	**FDR q**	**Enrichment**
Glycolytic process	3.66E-9	6.01E-6	19.00
Hypoxia-inducible factor-1alpha signaling pathway	1.70E-5	1.86E-3	47.65
Mitotic cell cycle process	1.63E-6	2.72E-4	2.11
Cell maturation	7.43E-4	3.4E-2	2.77

B. Gene Ontology Heat Maps

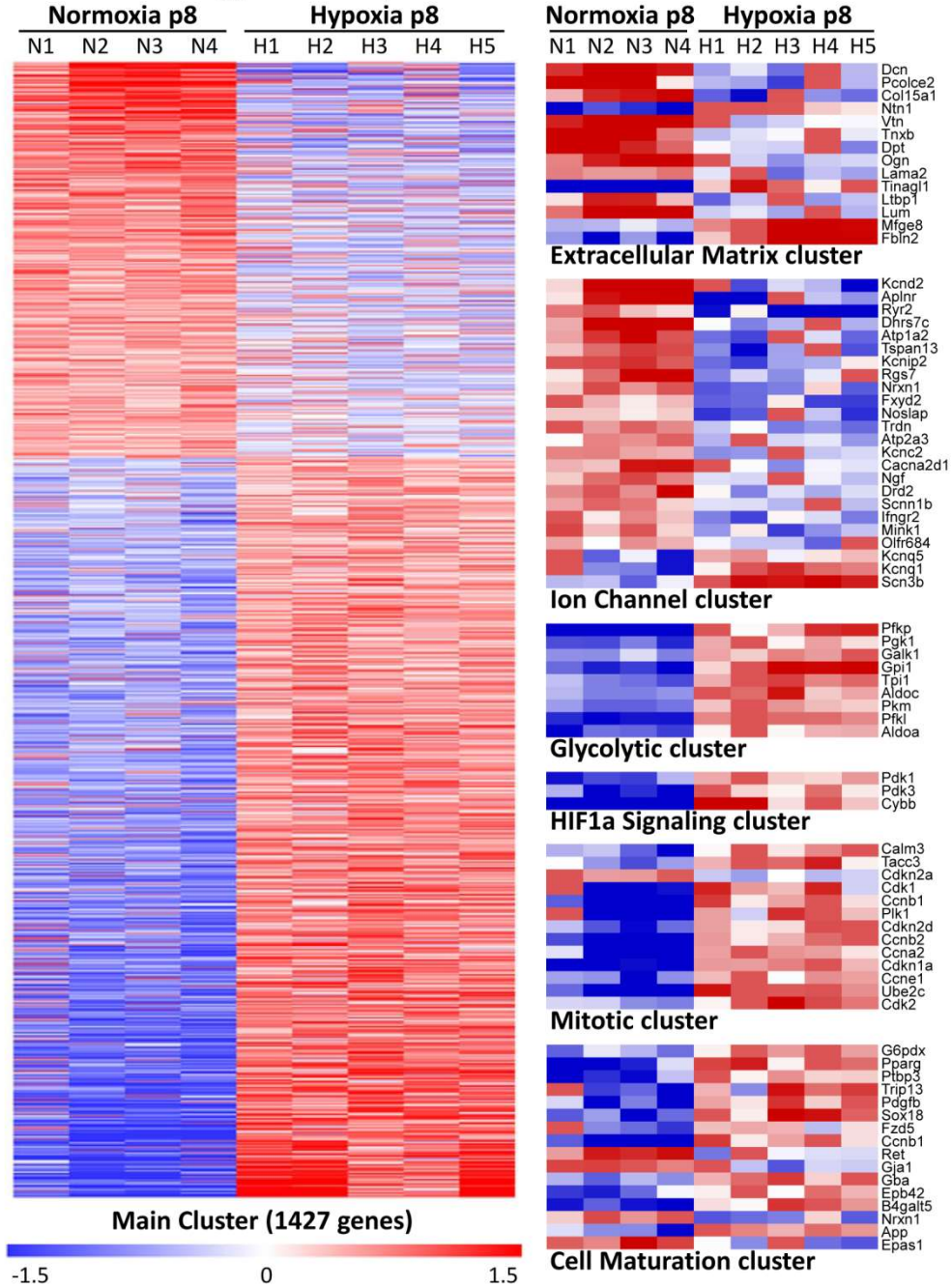

582

583 **Figure 4: Gene Ontologies. A:** Highlighted gene ontologies (GOs) important to cardiac
584 development and functioning that were different between groups at P8. **B:** Heat maps of the
585 main cluster of differentially expressed genes, as well as selected gene ontologies demonstrate
586 differential expression at P8 between groups. Each gene is median-centered, with data
587 displayed as fold-change.

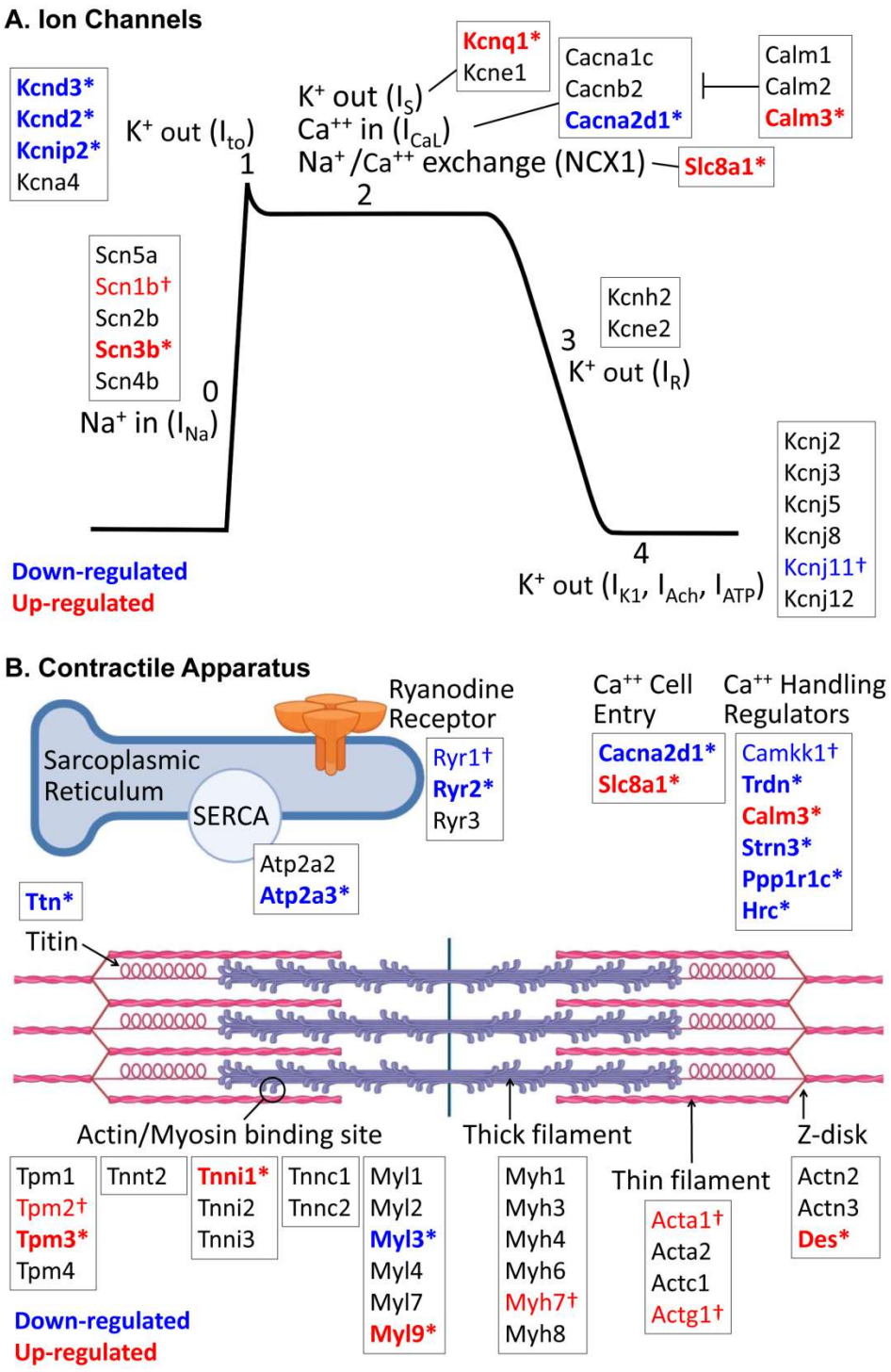

588

589 **Figure 5: Genes Affecting Ion Channels and the Contractile Apparatus. A:** At P8, hypoxia

590 affected genes involved with most phases of the cardiac action potential. **B:** Hypoxia affected

591 multiple genes important to the contractile apparatus, including both the sarcomere and calcium

592 handling machinery, at P8. *p≤0.05 and FDR q≤0.1 and †p≤0.05 and FDR q>0.1. Image

593 created with Biorender.com.

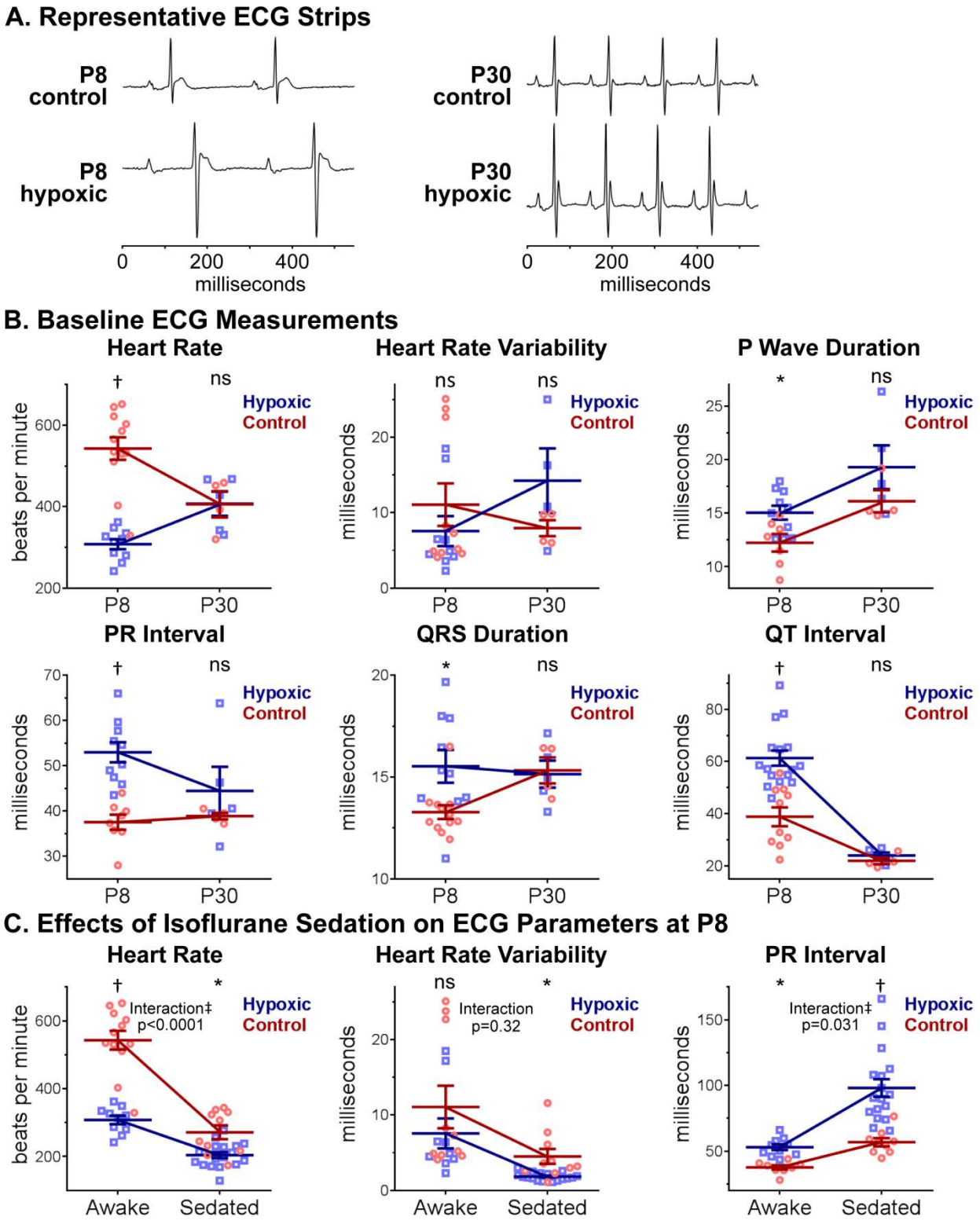

Figure 6: In-Vivo Electrocardiogram Measurements. A,B: Hypoxic P8 animals had lower heart rates compared to control, and hypoxia prolonged all ECG intervals measured, consistent

with slowed conduction speed. At P30, all ECG measurements had normalized. **C:** At P8, isoflurane sedation caused more PR prolongation in hypoxic animals than control. Data expressed as mean ± SEM. *p<0.05 hypoxic versus control. †p<0.0001 hypoxic versus control. ‡p<0.05 for two-way ANOVA interaction between sedation and group. ns=not significant.

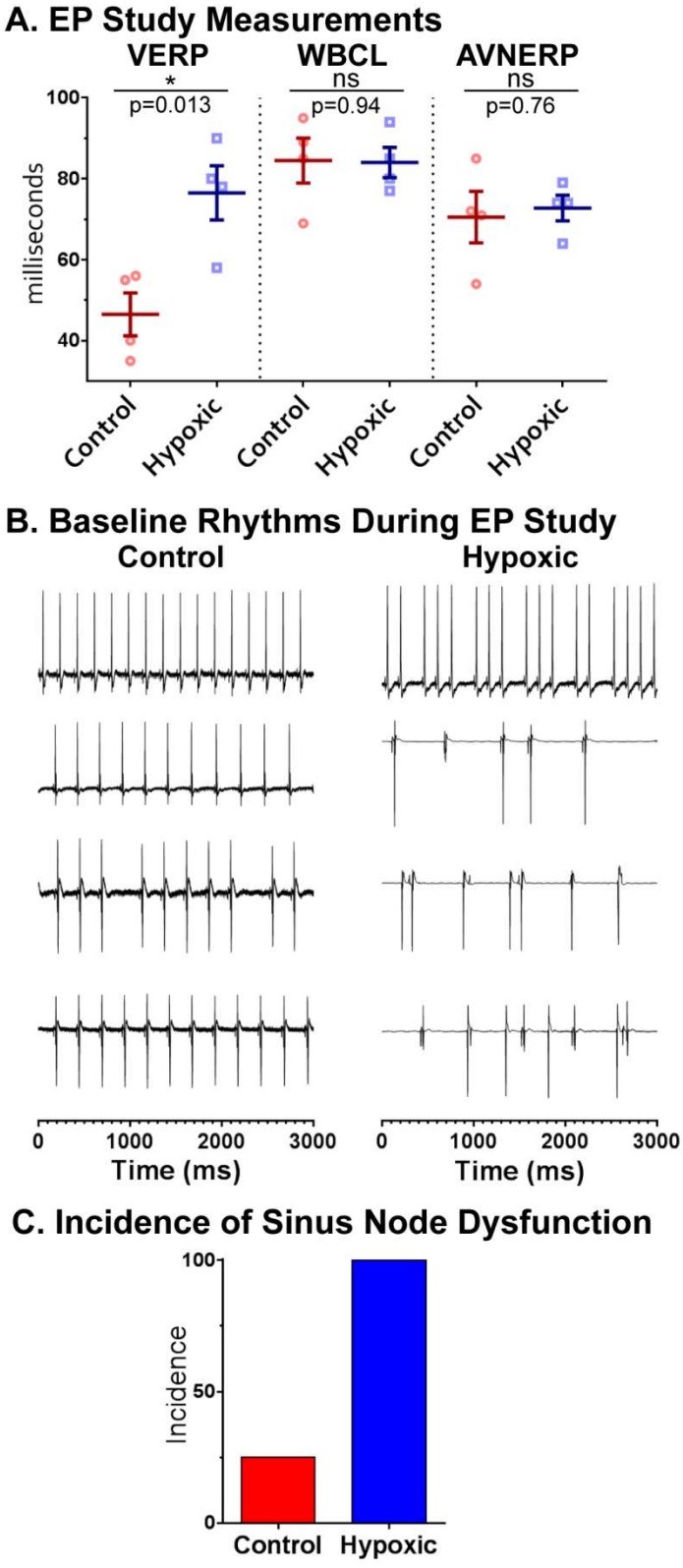

601

602 **Figure 7: Ex-Vivo Electrophysiology Study. A:** VERP was prolonged at P30 in animals

exposed to hypoxia. There was no difference for WBCL or AVNERP. **B:** Baseline rhythm during electrophysiology studies is displayed for each animal. **B, C:** 100% of hypoxic and 25% of control animals had sinus node dysfunction during the study. All data expressed as mean ± SEM. VERP, ventricular effective refractory period. WBCL, Wenckebach cycle length. AVNERP, atrioventricular nodal effective refractory period. *p<0.05. ns=not significant.

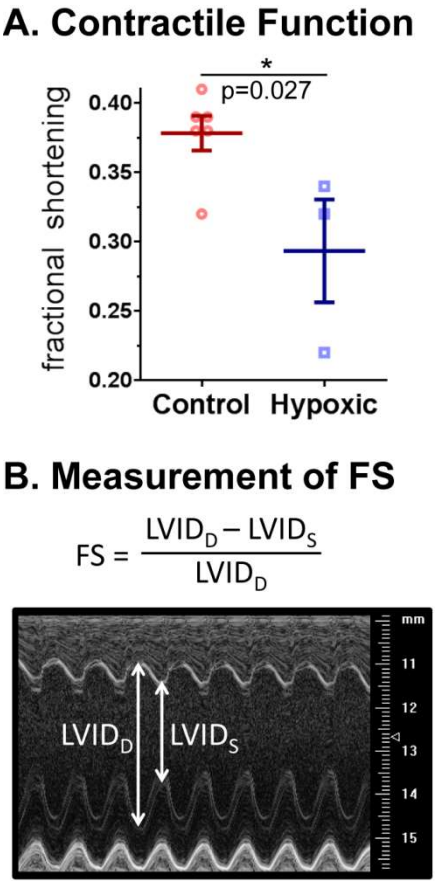

608

609 **Figure 8: Contractile Function. A:** Hypoxic animals had decreased contractile function

610 compared to control, as measured by fractional shortening (FS). **B:** Measurements of the left

611 ventricular internal diameter in systole ($LVID_S$) and diastole ($LVID_D$) were taken in M-Mode at

612 the level of the papillary muscles from a parasternal short axis view. VevoSonics 770 with

613 30MHz high frequency ultrasound probe. Data expressed as mean ± SEM. *p<0.05.